AIAA 99-3769

Vorticity Dynamics in a Porous Channel of the Closed-Closed Type. Part I: A Regular Perturbation Technique

Joseph Majdalani
Marquette University
Milwaukee, WI 53233

30th AIAA Fluid Dynamics Conference
18 June–1 July 1999
Norfolk, VA

Vorticity Dynamics in a Porous Channel of the Closed-Closed Type. Part I: A Regular Perturbation Technique

J. Majdalani*
Marquette University, Milwaukee, WI 53233

In the presence of time-harmonic pressure oscillations, the linearized Navier-Stokes equations have been solved to obtain an accurate description of the time-dependent field in a channel having a rectangular cross section and two equally permeable walls. Using regular perturbations, we present a closed form solution that becomes asymptotically exact as the kinetic Reynolds number increases indefinitely. We insist on verification and find that the validity of the asymptotics is strongly supported by evidence from numerical simulations. Furthermore, it appears that our formula embraces Stokes' exact solution when injection is suppressed. Indeed, when injection is reduced beyond the rigid wall diffusion speed, injection becomes insignificant, and we find our analytical formulation to agree favorably with the known exact solution. This reassuring observation is confirmed by quantifying the absolute error. The latter is found to exhibit a clear asymptotic behavior. Additionally, our analytical formulation reveals rich vortical structures and discloses the link between harmonic pressure oscillations and rotational waves. In the process, the explicit roles of variable injection, viscosity, and oscillation frequency are singled out.

I. Introduction

THIS paper is aimed at developing asymptotic formulations for the oscillatory flow field established inside a long and narrow rectangular channel where steady fluid transmission is permitted across a pair of counterfacing, permeable walls. The presumed oscillatory motion is instigated by self-excited harmonic pressure disturbances. The presence of intrinsic pressure oscillations can be ascribed, in practice, to the onset of a natural acoustic environment created, inevitably, by small fluctuations in the injectant rate at the porous walls. Undoubtedly, the strong coupling between oscillatory pressure gradients and bulk fluid motion entails rich structures that our model will attempt to capture. Aside from its pure scientific merit and relevance to fluid mechanists, the mathematical idealization to be pursued may have direct applications in rocket propulsion; namely, in understanding the unsteady flow character inside enclosures with transpiring walls. Since transpiring fluids can originate from slabs of burning propellant, surface ablation, phase sublimation, and ejection or withdrawal at solid boundaries, other possible applications include filtration, sweat and ablation cooling, dispensing of chemicals in cleaning facilities, gas diffusion in binary mixtures, and other membrane separation processes.

Consider, for example, the industrial separation of U_{235} from U_{238} by gaseous diffusion. This process involves vaporizing uranium and forcing the gaseous product through porous walls. Since differences in molecular weights cause dissimilar diffusion rates, the final concentration of a desired component depends, in part, on a judicious assessment of velocity and pressure distributions. Motivated by the need for economic product optimization, this practical application led Berman[1] to precipitate an ubiquitous study into a broad class of flows influenced by porous boundaries. To gain perspective on the problem at hand, some of these studies will be briefly reviewed.

Assuming a similarity transformation credited to Hiemenz,[2] Berman investigated the laminar, two-dimensional flow of a viscous incompressible fluid driven by uniform injection (or suction) in a rectangular channel with porous walls. Posing that the steady, normal velocity component is independent of the streamwise coordinate, he

*Assistant Professor, Department of Mechanical and Industrial Engineering. Member AIAA.

reduced the Navier-Stokes equations to a single, nonlinear, fourth-order, ordinary differential equation with four boundary conditions and a cross-flow Reynolds number R. The latter was based on the normal injection speed v_w and channel half-spacing h. For small R, he employed a regular perturbation scheme to derive an asymptotic formulation. In subsequent work, Berman[3] managed the same perturbative approach in the circular tube and annulus. Countless studies of channel flows with permeable walls followed.

For large suction, Sellars[4] obtained the first term of an approximation that was further expanded by Terrill,[5] who also extended Berman's small R case. Using an integral approach, Proudman[6] investigated the large R case with both equal and dissimilar injection or suction velocities. Using numerical curve-fitting principles, Morduchow[7] invoked, this time, the method of averages to arrive at simple approximations over the entire injection range. In contrast, White et al.[8] furnished, for any arbitrary R, an absolutely convergent power series whose coefficients were relegated to numerical trial-and-error routines.

For large injection, two contemporaneous and independently derived solutions were reported by Taylor,[9] and Yuan,[10] the former being a subset of the latter in the limiting case of an infinite R. A minor setback in Yuan's regular perturbation expansion was its inability to annex the viscous layer near the core, thus giving rise to singularities in its third derivative. This impediment was removed by Terrill[11] who employed matched asymptotic expansions to capture the inner layer.

Using regular perturbations, Terrill and Shrestha[12] also analyzed electrically conducting fluids, injected or extracted at low R, in the presence of a transverse magnetic field. For large R, Shrestha[13] employed matched asymptotic expansions in treating the corresponding magnetohydrodynamical problem.

For unsymmetrical flows brought about by different wall permeabilities, injection or suction velocities, Terrill and Shrestha[14] constructed a generalized perturbation series for small R. For large injection, Shrestha and Terrill[15] extended Proudman's one-term expression using the method of inner and outer expansions. In continuation of asymmetric solutions, Cox[16] tackled, years later, the practically attractive case of an impermeable wall counterfacing a transpiring wall by relying on numerical simulations to support matched asymptotic predictions.

Spurred on by the need to study long slender droplets trapped in extensional flows, Brady and Acrivos[17] presented an exact solution to the Navier-Stokes equations for a flow driven by an accelerating surface velocity and symmetric boundary conditions. When the accelerating walls were made permeable, a purely academic formulation was addressed by Watson et al.[18]. The latter generalized previous work by incorporating both coupled mechanisms in constructing asymptotic expansions for small and large R. In the same context, the case of asymmetrically accelerating walls was examined by Watson[19] as well.

The spatial stability of steady solutions of the Berman family was considered by several authors, including Varapaev and Yagodkin,[20] Raithby and Knudsen,[21] Hocking,[22] Sviridenkov and Yagodkin,[23] Brady,[24] and Durlofsky and Brady.[25] Some of their results suggested that injection flows tended to be absolutely stable and well-behaved, asymptotically in R, and that increasing R reduced the steady flow development length. Conversely, suction flows appeared to be more amenable to instability and reversal, exhibiting inflection points and dual solutions in some ranges of R.

For over two decades now, the daunting proof of solution multiplicity at different R values seems to have attracted intensive labors from several workers. To name a few, we cite Robinson[26], Skalak and Wang[27], Shih,[28] Hastings et al.,[29] Lu et al.,[30] MacGillvray and Lu,[31] and Lu.[32] Insofar as injection is concerned, both Shih[28] and Hastings et al.,[29] the latter using a simpler approach, were able to prove irrevocably the existence of a unique solution for all R, a conclusion noted previously, without rigorous proof, by Skalak and Wang.[27]

Recently, the temporal stability of such flows has received attention vis-à-vis studies made by Zaturska et al.,[33] Taylor et al.,[34] and Watson et al.[18,19] Among other deliberations, such studies ascertained that steady symmetric flows corresponding to the wall injection type were stable to time-dependent perturbations.

While the majority of studies, recounted earlier, relied on numerical simulations for validation purposes, some drew conclusions from experimental observations. Confirmatory laboratory experiments on steady channel flow through porous sheets conducted by Taylor,[9] Varapaev and Yagodkin,[20] Raithby and Knudsen,[21] and Sviridenkov and Yagodkin[23] indicated that Taylor's or Yuan's similarity solutions with injection were indeed observed to develop rapidly within the channel.

The addition of longitudinal pressure oscillations in channels with plane porous walls was achieved experimentally by Ma et al.,[35,36] Barron et al.,[37] Avalon et al.[38] and Casalis et al.[39] Both Ma and Barron borrowed the concept of producing an alternating flow by external means from Richardson and Tyler[40] who used electric motors to control the reciprocating motion of a piston mounted at the end of a crank. Naturally, the to-and-fro piston motion caused the transpiring gas inside the channel to vibrate harmonically. The main disparity between Ma's apparatus and Barron's is that the latter used a Scotch-yoke to drive the piston, which resulted in pure sinusoidal piston displacements. This, of course, constituted an improvement over Ma's slider-crank mechanism which produced undesirable harmonics. In both instances, carbon dioxide was expelled from flat blocks of sublimating dry ice to simulate the injectant. More recently, Avalon et al.[38] and Casalis et al.[39] demonstrated the existence of intrinsic, self-induced harmonic oscillations in their 'VECLA' facility which comprised a long channel with two counterfacing permeable and impermeable walls. As uniform air injection was maintained through the plane porous sections of their apparatus, small unavoidable fluctuations in the injectant rate led decidedly to the onset of a strong acoustic environment. In all three experiments, the placement of a choked orifice or nozzle at the downstream end determined whether or not the oscillation mode character was of the closed-closed or closed-open type. In the current paper, we shall focus on the basic laminar flow model that corresponds to pressure oscillations of the closed-closed type.

The objective will be, therefore, to derive an accurate asymptotic solution to the two-dimensional oscillatory field in a channel with plane porous walls using successive approximations. We hope that the detailed knowledge we seek will help develop physical intuition into more realistic flows in channels and tubes.

The forthcoming treatment is organized in the following manner. We start in Sec. II by defining the geometry at hand, Berman's mean flow solution, and pertinent assumptions. This is followed in Sec. III by linearizing the Navier-Stokes equations via regular perturbations in the injection Mach number and harmonic pressure amplitude. In Sec. IV we invoke a powerful theorem that permits decomposing the time-dependent field into irrotational and solenoidal components. Whereas the irrotational, pressure-driven solution can be obtained rather straightforwardly, the solenoidal, vorticity-driven component demands a careful treatment and is deferred to Sec. V. Hence Sec. V constitutes the heart of the analysis wherein new formulations are delivered. Results are compared to numerical solutions of the linearized Navier-Stokes equations in Sec. VI. In the process, the time-dependent vortical structure is closely examined along with the error associated with the asymptotic formulas. Since one would expect the transpiring walls to become inactive when injection is suppressed, our asymptotic formulation is compared to the corresponding exact solution of the Stokes type for a plane, periodic flow between parallel walls. By way of closure, we retire with concluding remarks in Sec. VII.

II. Model Description

A. Geometry

The flow to be studied takes place in a long rectangular channel of length L and width w, bounded by plane porous walls that are $2h$ apart. Through these walls, a Newtonian fluid is injected with constant uniform velocity v_w. In this paper, we shall, in fact, limit our attention to a perfect gas. Taking one side of the cross section to be smaller than the other two enables us to treat the problem as a case of two-dimensional flow. We note parenthetically that it has been demonstrated by Terrill[5] (cf. p. 309-310) that the ratio of the width to the height of the channel does not have to be large to justify ignoring the influence of passive side walls. Accordingly, a ratio of $w/h \geq 4$ is reasonably large enough. When both channel walls are taken to have equal permeability, one can assume perfect symmetry about a plane midway between the walls. Symmetry reduces the solution domain by half, making it sufficient to investigate the flow behavior over half of the channel, extending from

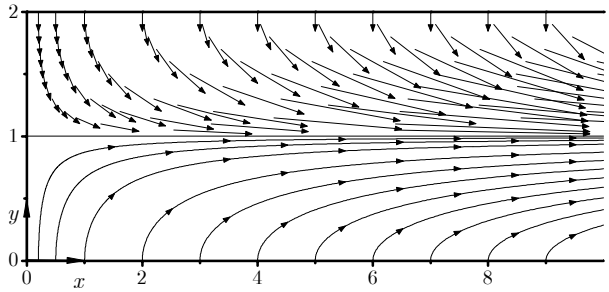

Fig. 1 Mean flow streamlines shown in the bottom half of the domain counterfacing a vector plot in the opposite half.

one permeable wall to the meridian plane. As shown schematically in Fig. 1, a coordinate system can be chosen with the origin at the porous wall. After normalizing all spatial coordinates by h, the streamwise, transverse, and spanwise coordinates are denoted by x, y, and z, respectively. The benefit of selecting y to be the normal distance measured from the wall will materialize in later discussions of boundary layer issues. Disregarding the influence of rigid boundaries, we assume no variations in z and confine our solution to $0 \le x \le l$, and $0 \le y \le 1$, where $l = L/h$.

When the channel is closed at the head end and choked at the downstream end, small fluctuations in the injectant rate give rise to harmonic pressure oscillations. These small pressure fluctuations can, in turn, couple with the mean flow and give rise to a time-dependent field that we wish to investigate. The streamlines depicted in Fig. 1 correspond to typical flow patterns pertaining to the undisturbed state.

B. Criteria

In managing a closed-form solution, several criteria must be met. In connection with the mean flow motion, we demand that steady conditions prevail in a laminar, rotational, and incompressible regime where neither swirling nor mixing between incoming streams can take place. After ignoring external gravitational or electromagnetic forces, the condition of uniform porosity is simulated by prescribing a constant normal velocity at the wall that is independent of position. On the one hand, we limit our scope to cross-flow Reynolds numbers satisfying $R = v_w h/\nu > 20$, where ν is the kinematic viscosity. The advantage is that, in this range, the mean flow can be adequately expressed by the well-known Taylor solution, which offers substantial mathematical simplifications on route to extracting a time-dependent solution. The upper limit imposed on R is decreed, on the other hand, by the need to maintain an injection Mach number $M = v_w/a_s$ of order 10^{-3}, with a_s referring to the stagnation speed of sound. The reason is this. In linearizing the Navier-Stokes equations, we shall employ M as a perturbation parameter. Consequently, our final formulation will entail an error of $\mathcal{O}(M)$. Since a_s far exceeds v_w in most applications, M will be very small in practice.

In what concerns the time-harmonic field performing small oscillations about the base flow, we constrain the oscillatory pressure amplitude A to remain small by comparison to the stagnation pressure p_s evaluated at $x = 0$. This enables us to construct another small parameter that scales with A/p_s. Since the mean pressure depreciates in the streamwise direction, we limit the channel length to $l < 100$, for consistency in perturbation levels. Finally, in order to break down the analysis into digestible pieces, we assume that the presence of isentropic oscillations does not affect the bulk fluid motion.

C. Mean Flow Definition

In the absence of harmonic disturbances, the Navier-Stokes equations can be solved exactly using a similarity transformation. As demonstrated by Berman,[1] when the steady stream function Ψ varies linearly in the streamwise direction, viz. $\Psi = -xF(y)$, one can write (cf. Varapaev[20] or Proudman[6]), $(u_0, v_0) = (-xF', F)$, where $\boldsymbol{u}_0 = (u_0, v_0)$ is the mean velocity vector normalized by v_w. The separable component F must satisfy Berman's equation, $F^{iv} + R(F'F'' - FF''') = 0$, which depends on R (> 0 for injection) and four boundary conditions: $F'(0) = F(1) = F''(1) = 0$, and $F(0) = 1$. Although it is possible to manage a time-dependent formulation for arbitrary F, we incline to use a simple and practical solution corresponding to $F = \cos(\frac{\pi}{2} y)$, which becomes exact as $R \to \infty$. More sophisticated Berman functions can give rise to technical issues that tend to complicate and slightly obscure the upcoming analysis. This ideal solution, attributed to Taylor,[9] has been thoroughly verified both numerically and experimentally to be a reasonable approximation for $R > 20$. In this range, Varapaev[20] notes minimal solution changes and almost no changes for $R > 100$. With this choice of F, the velocity and vorticity fields are expressible by

$$\boldsymbol{u}_0 = (\tfrac{\pi}{2} x \sin(\tfrac{\pi}{2} y), \cos(\tfrac{\pi}{2} y)), \quad \omega_0 = -\tfrac{\pi^2}{4} x \cos(\tfrac{\pi}{2} y) \qquad (2.1)$$

which satisfy all the boundary conditions, including the no-slip at the wall. After normalizing the mean pressure by γp_s, (where γ is the ratio of specific heats), one can integrate the ideal momentum equation to get

$$p_0(x, y) = 1/\gamma - M^2 \left[\tfrac{\pi^2}{4} x^2 + \cos^2(\tfrac{\pi}{2} y)\right]/2 . \qquad (2.2)$$

The last formula makes it abundantly clear that the error associated with a uniform mean pressure assumption will be less than a few percent when $x \le 100$. Were it not for this limitation, our

analysis would have been applicable to a semi-infinite channel.

III. Linearized Navier-Stokes Equations

A. Fundamental Equations

Assuming constant kinematic viscosity and negligible bulk viscosity, the differential conservation of mass and momentum can be cast into the familiar nondimensional form

$$\partial\hat{\rho} / \partial t + \nabla.(\hat{\rho}\hat{\boldsymbol{u}}) = 0\,, \tag{3.1}$$

$$\hat{\rho}\left[\partial\hat{\boldsymbol{u}} / \partial t + (\hat{\boldsymbol{u}}.\nabla)\hat{\boldsymbol{u}}\right] = -\nabla\hat{p} + \overline{R}^{-1}\left[4\nabla(\nabla.\hat{\boldsymbol{u}}) / 3 - \nabla\times(\nabla\times\hat{\boldsymbol{u}})\right], \tag{3.2}$$

where the total instantaneous velocity $\hat{\boldsymbol{u}}$ is normalized by the speed of sound a_s, spatial coordinates by h, and time is made dimensionless by reference to h / a_s, the average time it takes for a pressure disturbance to travel from the wall to the core. Using asterisks for dimensional variables, the instantaneous pressure and density can be referenced to stagnation conditions. Setting $\hat{p} \equiv \hat{p}^* / (\gamma p_s)$, $\hat{\rho} \equiv \hat{\rho}^* / \rho_s$, the acoustic Reynolds number $\overline{R}$ that appears in (3.2) will be $a_s h / \nu$.

B. Variable Decomposition

When periodic oscillations are introduced at a radian frequency k, the instantaneous pressure can be written as a sum of its steady and fluctuating components. Using subscripts for perturbation orders, the total pressure can be expanded into

$$\begin{aligned}\hat{p}^* &= p_0^*(x^*,y^*) + p_1^*(x^*,y^*,t^*)\\ &= p_0^* + AP(x^*,y^*)\exp(-\mathrm{i}kt^*)\,,\end{aligned} \tag{3.3}$$

where P is a spatial function of $\mathcal{O}(1)$ that will be determined in Sec. IV(D). Normalizing and using $p_0^* = p_s$, we get

$$\begin{aligned}\hat{p}(x,y,t) &= 1/\gamma + \bar{\varepsilon}P(x,y)\exp(-\mathrm{i}k_m t) + \mathcal{O}(M^2x^2)\\ &\cong 1/\gamma + \bar{\varepsilon}p_1(x,y,t)\,,\end{aligned} \tag{3.4}$$

where $k_m = kh / a_s$ is the nondimensional frequency, and $\bar{\varepsilon} = A / (\gamma p_s)$ is the wave amplitude, a gauge parameter that provides a scale to which other quantities can be compared. Other fluctuating variables can be expanded in a similar fashion. For example, one can define $\rho_1^* \equiv \bar{\varepsilon}\rho_s\rho_1$, and $\boldsymbol{u}_1^* \equiv \bar{\varepsilon}a_s\boldsymbol{u}_1$, where ρ_1 and $\boldsymbol{u}_1$ are time-dependent functions of $\mathcal{O}(1)$ that can be later evaluated. At the outset, one can write

$$\hat{\rho}(x,y,t) = (\rho_s + \rho_1^*) / \rho_s = 1 + \bar{\varepsilon}\rho_1(x,y,t)\,. \tag{3.5}$$

In much the same way, velocity lends itself to decomposition. Knowing the mean solution from (2.1) and (2.2), we may follow Lighthill[41] by assuming small velocity oscillations about the mean and expand the dimensional velocity as

$$\begin{aligned}\hat{\boldsymbol{u}}^*(x^*,y^*,t^*) &= \boldsymbol{u}_0^*(x^*,y^*) + \boldsymbol{u}_1^*(x^*,y^*,t^*)\\ &= v_w\boldsymbol{u}_0(x^*,y^*) + \boldsymbol{u}_1^*(x^*,y^*,t^*)\,.\end{aligned} \tag{3.6}$$

Normalizing by a_s begets, for the velocity and vorticity companion,

$$\hat{\boldsymbol{u}}(x,y,t) = M\boldsymbol{u}_0(x,y) + \bar{\varepsilon}\,\boldsymbol{u}_1(x,y,t)\,,$$

$$\text{and}\qquad \hat{\boldsymbol{\omega}}(x,y,t) = M\boldsymbol{\omega}_0(x,y) + \bar{\varepsilon}\boldsymbol{\omega}_1(x,y,t)\,. \tag{3.7}$$

C. Linearization

Inserting (3.4) through (3.7) back into (3.1)-(3.2) precipitates the zero order expansion in the wave amplitude which is already satisfied by the mean flow. Collecting terms of $\mathcal{O}(\bar{\varepsilon})$, the first order linearized expansion of the fundamental equations is attained:

$$\partial\rho_1 / \partial t + \nabla\cdot\boldsymbol{u}_1 = -M\nabla\cdot(\rho_1\boldsymbol{u}_0)\,, \tag{3.8}$$

$$\begin{aligned}&\partial\boldsymbol{u}_1 / \partial t\\ &= -M\left[\nabla(\boldsymbol{u}_0\cdot\boldsymbol{u}_1) - \boldsymbol{u}_1\times(\nabla\times\boldsymbol{u}_0) - \boldsymbol{u}_0\times(\nabla\times\boldsymbol{u}_1)\right]\\ &\quad -\nabla p_1 + \overline{R}^{-1}\left[4\nabla(\nabla\cdot\boldsymbol{u}_1)/3 - \nabla\times(\nabla\times\boldsymbol{u}_1)\right].\end{aligned} \tag{3.9}$$

This set encapsulates the implicit influence of bulk fluid motion on the time-dependent field. The reader unfamiliar with this set may, if so inclined, derive it straight-forwardly or apply to the author for a typescript.

IV. Vector Superposition

A. Flow Field Decomposition

It proves expedient to decompose the time-dependent vector into an irrotational and a solenoidal component, the former being the gradient of a scalar s, and the latter being the curl of a vector $\boldsymbol{q}$. This notion correlates to a known mathematical theorem cited in Sommerfeld,[42] which can be used to synthesize the total harmonic disturbance out of two components associated with irrotational, pressure-driven, and solenoidal, vorticity-driven modes. Using a circumflex to designate irrotational parts, and a tilde for solenoidal parts, the time-dependent velocity can be expressed as

$$\boldsymbol{u}_1 = \hat{\boldsymbol{u}} + \tilde{\boldsymbol{u}} \equiv \nabla s + \nabla\times\boldsymbol{q}\,. \tag{4.1}$$

Evidently, $\nabla\times\hat{\boldsymbol{u}} = 0$, and $\nabla\cdot\tilde{\boldsymbol{u}} = 0$. Similar decomposition of a small disturbance into pressure and vorticity modes has been effectuated

previously by numerous authors, including Chu and Kovásznay,[43] Carrier and Carlson,[44] and others. Then, by definition,

$$\boldsymbol{\omega}_1 \equiv \nabla \times \boldsymbol{u}_1 = \tilde{\boldsymbol{\omega}} \equiv \nabla \times \tilde{\boldsymbol{u}} \ , \ p_1 = \hat{p} \ , \ \rho_1 = \hat{\rho} \ . \quad (4.2)$$

In other words, time-dependent vorticity is ascribed to the rotational mode and harmonic pressure is associated with the irrotational mode. The pseudo-pressure arising in the vortical mode analysis can be safely dismissed, being of second order. The last term in (4.2) stems from the known relation, $\hat{p} = \hat{\rho}$, for a perfect gas undergoing isentropic oscillations.

B. Splitting the Navier-Stokes Equations

When (4.1)-(4.2) are substituted back into (3.8)-(3.9), two independent sets of formulas ensue. These are coupled through existing boundary conditions and are given by

1. Irrotational Set

$$\partial \hat{\rho} \,/\, \partial t + \nabla \cdot \hat{\boldsymbol{u}} = -M \nabla \cdot (\hat{\rho} \boldsymbol{u}_0) \,, \quad (4.3)$$

$$\partial \hat{\boldsymbol{u}} \,/\, \partial t = -\nabla \hat{p} \,/\, \gamma + 4 \overline{R}^{-1} \nabla (\nabla \cdot \hat{\boldsymbol{u}}) \,/\, 3 - M \Big[\nabla (\hat{\boldsymbol{u}} \cdot \boldsymbol{u}_0) - \hat{\boldsymbol{u}} \times (\nabla \times \boldsymbol{u}_0) \Big] . \quad (4.4)$$

2. Solenoidal Set

$$\nabla \cdot \tilde{\boldsymbol{u}} = 0 \,, \quad (4.5)$$

$$\partial \tilde{\boldsymbol{u}} \,/\, \partial t = -\overline{R}^{-1} \nabla \times (\nabla \times \tilde{\boldsymbol{u}}) - M \Big[\nabla (\tilde{\boldsymbol{u}} \cdot \boldsymbol{u}_0) - \tilde{\boldsymbol{u}} \times (\nabla \times \boldsymbol{u}_0) - \boldsymbol{u}_0 \times (\nabla \times \tilde{\boldsymbol{u}}) \Big] . \quad (4.6)$$

C. Auxiliary Conditions

In attaining $\boldsymbol{u}_1$, both $\hat{\boldsymbol{u}}$ and $\tilde{\boldsymbol{u}}$ must be first determined and then superposed in a manner to correctly satisfy two auxiliary conditions: velocity adherence at the wall demanding that $u_1(x, 0) = 0$, or $\hat{u}(x, 0) + \tilde{u}(x, 0) = 0$, and symmetry at $y = 1$ requiring that $\partial u_1(x, 1) \,/\, \partial y = 0$.

D. Irrotational Solution

When $\hat{p} = \hat{\rho}$ is utilized, standard manipulation of (4.3)-(4.4) condenses the set into a single hyperbolic partial differential equation,

$$\partial^2 \hat{p} \,/\, \partial t^2 - \nabla^2 \hat{p} = -M \left\{ \nabla \cdot (\boldsymbol{u}_0 \partial \hat{p} \,/\, \partial t) - \nabla^2 (\hat{\boldsymbol{u}} \cdot \boldsymbol{u}_0) + \nabla \cdot \big[\hat{\boldsymbol{u}} \times (\nabla \times \boldsymbol{u}_0) \big] \right\} . \quad (4.7)$$

At this juncture, a solution can be managed to $\mathcal{O}(M)$ by applying separation of variables and the rigid wall boundary conditions. Since $l >> 1$, the lowest naturally excited frequencies will correspond to the least damped longitudinal oscillation modes, making it safe to neglect transverse modes of higher frequencies. In practice, laboratory experiments confirm that low oscillation modes tend to dominate because lower modes require less energy to excite. For axial harmonic waves in a long channel with constant cross section, a solution to (4.7) can be retrieved from most textbooks on wave propagation. Expressed in Euler's notation, the harmonic pressure reads

$$\hat{p}(x, t) = \cos(k_m x) \exp(-\mathrm{i} k_m t) + \mathcal{O}(M) \,, \quad (4.8)$$

where the dimensionless wave number is given by $k_m = kh \,/\, a_s = m\pi \,/\, l$, $m = 1, 2, 3, \ldots$; m being the oscillation mode number. The velocity companion can be integrated from (4.4) to render

$$\hat{\boldsymbol{u}}(x, t) = \mathrm{i} \sin(k_m x) \exp(-\mathrm{i} k_m t) \boldsymbol{i} + \mathcal{O}(M) \,. \quad (4.9)$$

E. Solenoidal Equations

Letting $\overline{\boldsymbol{u}}(x, y) \equiv (\overline{u}, \overline{v})$, and $\overline{\boldsymbol{\omega}} \equiv \nabla \times \overline{\boldsymbol{u}} = \overline{\omega} \boldsymbol{k}$, we use Euler's notation and write the vortical fluctuations as

$$\tilde{\boldsymbol{u}}(x, y, t) = \overline{\boldsymbol{u}}(x, y) \exp(-\mathrm{i} k_m t) \,,$$
$$\tilde{\boldsymbol{\omega}}(x, y, t) = \overline{\boldsymbol{\omega}}(x, y) \exp(-\mathrm{i} k_m t) \,. \quad (4.10)$$

In lieu of (4.5)-(4.6), we now have

$$\nabla \cdot \overline{\boldsymbol{u}} = 0 \,, \quad (4.11)$$

$$\mathrm{i} \overline{\boldsymbol{u}} = \Big[\nabla (\overline{\boldsymbol{u}} \cdot \boldsymbol{u}_0) - \overline{\boldsymbol{u}} \times \boldsymbol{\omega}_0 - \boldsymbol{u}_0 \times \overline{\boldsymbol{\omega}} \Big] \,/\, S + \nabla \times \overline{\boldsymbol{\omega}} \,/\, K \,, \quad (4.12)$$

where

$$S = \frac{k_m}{M} = \frac{kh}{v_w} \,, \text{ and } K = \frac{kh^2}{\nu} = \frac{h^2}{(\sqrt{\nu \,/\, k})^2} \,. \quad (4.13)$$

The two emerging similarity parameters are the Strouhal number S, and the kinetic Reynolds number K, each representing the quotient of time-dependent inertia to either mean flow convection or diffusion. Practically, since the kinematic viscosity of most gases happens to be very small, the parametric variation in K reported by many researchers has fallen into the range $10^4 < K < 10^8$. On that account, we define $\varepsilon \equiv K^{-1}$ to be a primary perturbation parameter. For similar reasons, since unsteady flows are characterized by appreciable Strouhal numbers, we define $\sigma = 1 \,/\, S$. We note that ε is always smaller than σ since the ratio $\sigma \,/\, \varepsilon = v_w h \,/\, \nu$ is the cross-flow Reynolds number R, which is large irrespective of frequency.

Subject to confirmation at the conclusion of the forthcoming asymptotic analysis, we now make the

conditional stipulation that $\overline{v}/\overline{u} = \mathcal{O}(M)$. This *proviso* is necessary to forge ahead with the leading-order approximation. Being a smaller quantity, $\overline{v}$ can be omitted at the first perturbation level with no effect on the solution desired at $\mathcal{O}(M)$. On that account, (4.12) collapses at $\mathcal{O}(M)$ into

$$\mathrm{i}\overline{u} = \sigma\left[\frac{\partial}{\partial x}(\overline{u}u_0) + v_0\frac{\partial\overline{u}}{\partial y}\right] - \varepsilon\frac{\partial^2\overline{u}}{\partial y^2},$$

or

$$\mathrm{i}\overline{u} = \sigma\left[\frac{\partial}{\partial x}(\overline{u}u_0) - v_0\overline{\omega}\right] + \varepsilon\frac{\partial\overline{\omega}}{\partial y}. \qquad (4.14)$$

V. Solenoidal Field

A. Vorticity Transport Equation

Taking the curl of (4.12) and using (4.10), the vorticity transport equation emerges:

$$\mathrm{i}\overline{\boldsymbol{\omega}} = -\sigma\nabla\times(\overline{\boldsymbol{u}}\times\boldsymbol{\omega}_0 + \boldsymbol{u}_0\times\overline{\boldsymbol{\omega}}) - \varepsilon\nabla^2\overline{\boldsymbol{\omega}} + \mathcal{O}(M) \qquad (5.1)$$

This can be rearranged in a scalar form that places leading-order terms on the left-hand side:

$$\frac{\partial\overline{\omega}}{\partial y} - \frac{\mathrm{i}\overline{\omega}}{\sigma v_0} + \frac{u_0}{v_0}\frac{\partial\overline{\omega}}{\partial x} = -\frac{\overline{u}}{v_0}\frac{\partial\omega_0}{\partial x} + \frac{\varepsilon}{\sigma v_0}\left(\frac{\partial^2\overline{\omega}}{\partial x^2} + \frac{\partial^2\overline{\omega}}{\partial y^2}\right) \qquad (5.2)$$

The right-hand side quantities representing the steady vorticity gradient and the viscous diffusion of time-dependent vorticity can be ignored at the first perturbation level. This can be justified by stretching the normal scale over the Mach number range. Introducing momentarily the magnified scale $Y = y/M$ into (5.2) yields

$$\frac{\partial\overline{\omega}}{\partial \mathrm{Y}} - \frac{\mathrm{i}k_m\overline{\omega}}{v_0} + M\frac{u_0}{v_0}\frac{\partial\overline{\omega}}{\partial x} = -M\frac{\overline{u}}{v_0}\frac{\partial\omega_0}{\partial x} + \frac{1}{v_0\overline{R}}\left(\frac{1}{M^2}\frac{\partial^2\overline{\omega}}{\partial \mathrm{Y}^2} + \frac{\partial^2\overline{\omega}}{\partial x^2}\right). \qquad (5.3)$$

Thus it can be argued that, since the right-hand side of (5.3) contains terms of $\mathcal{O}(M)$ and smaller, subsequent leading-order expansions in M will not be affected by their presence. Physically, these terms symbolize viscous dissipation and axial convection of mean flow vorticity by virtue of the time-dependent vortical action. The latter is insignificant because of our original stipulation restricting unsteady flow effects on mean flow parameters to remain marginal. The third term on the left-hand side is retained, despite its misleading appearance of $\mathcal{O}(M)$, because it represents the downstream convection of vorticity. This phenomenon is vital to preserve two-dimensional physics by providing an outlet to incoming vorticity. The base solution can now be achieved by expanding $\overline{\omega}$ in powers of M, viz., $\overline{\omega} = \varpi_0 + M\varpi_1 + \mathcal{O}(M^2)$. Following substitution into (5.2), the leading-order term can be retrieved, by separation of variables, from

$$\frac{\partial\varpi_0}{\partial y} - \frac{\mathrm{i}\varpi_0}{\sigma v_0} + \frac{u_0}{v_0}\frac{\partial\varpi_0}{\partial x} = 0. \qquad (5.4)$$

This, of course, must be contingent upon satisfaction of both the no-slip condition at the wall, and the no-flow restriction at the head end. Letting $\varpi_0 = X(x)Y(y)$, (5.4) becomes

$$\frac{x}{X}\frac{\mathrm{d}X}{\mathrm{d}x} = -\frac{2}{\pi}\cot\left(\frac{\pi}{2}y\right)\frac{1}{Y}\frac{\mathrm{d}Y}{\mathrm{d}y} + \frac{2\mathrm{i}}{\pi\sigma}\csc\left(\frac{\pi}{2}y\right) = \lambda_n, \qquad (5.5)$$

where λ_n must be a strictly positive real number for a nontrivial solution. Integrating and summing linearly over all possible solutions yields

$$\varpi_0 = \sum_{\lambda_n} c_n\left[x\cos\left(\frac{\pi}{2}y\right)\right]^{\lambda_n}\exp\left\{\frac{2\mathrm{i}}{\pi\sigma}\ln\tan\left[\frac{\pi}{4}(1+y)\right]\right\} \qquad (5.6)$$

where ϖ_0 contains a denumerable set of arbitrary constants c_n associated with each λ_n. These must be specified in a manner to satisfy the no-slip condition at the wall, written for vorticity. The latter requires a delicate treatment and shall be addressed separately.

B. Pressure-Driven Vorticity

It is instructive to reduce (3.9), vis-à-vis our current state of knowledge, into

$$\partial\boldsymbol{u}_1/\partial t = -M\left[\nabla(\boldsymbol{u}_1\cdot\boldsymbol{u}_0) - \boldsymbol{u}_1\times\boldsymbol{\omega}_0 - \boldsymbol{u}_0\times\boldsymbol{\omega}_1\right] - \nabla p_1 - \overline{R}^{-1}\nabla\times\boldsymbol{\omega}_1, \qquad (5.7)$$

whose projection along x reads

$$\frac{\partial u_1}{\partial t} = -M\left[\frac{\partial}{\partial x}(u_0u_1 + v_0v_1) - v_1\omega_0 - v_0\omega_1\right] - \frac{\partial p_1}{\partial x} - \frac{1}{\overline{R}}\frac{\partial\omega_1}{\partial y}. \qquad (5.8)$$

Recalling that $\omega_1 = \tilde{\omega}$, $v_1 = \tilde{v}$, $p_1 = \hat{p}$, and that $u_1(x,0,t)$ must vanish to prevent slippage, (5.8) collapses, at the wall, into

$$0 = -M\left[\frac{\partial}{\partial x}(\tilde{v}v_0) - \tilde{v}\omega_0 - v_0\tilde{\omega}\right] - \frac{\partial\hat{p}}{\partial x} - \frac{1}{\overline{R}}\frac{\partial\tilde{\omega}}{\partial y} \qquad (5.9)$$

Rearranging, and using $\hat{p} = \cos(k_m x)\exp(-\mathrm{i}k_m t)$, the no-slippage translates into

$$\tilde{\omega} = \frac{1}{M}\frac{\partial\hat{p}}{\partial x} + \frac{\varepsilon}{\sigma}\frac{\partial\tilde{\omega}}{\partial y} + \frac{\partial\tilde{v}}{\partial x} + \frac{\pi^2}{4}x\tilde{v} = -S\sin(k_m x)\exp(-\mathrm{i}k_m t) + \frac{1}{R}\frac{\partial\tilde{\omega}}{\partial y} + \mathcal{O}(M), \qquad (5.10)$$

which can be recast into

$$\overline{\omega}(x,0) = -S\sin(k_m x) + \frac{1}{R}\frac{\partial\overline{\omega}}{\partial y} + \mathcal{O}(M)\,. \quad (5.11)$$

Equation (5.11) indicates that 'fresh' vorticity owes its origin at the wall to the oscillatory pressure gradient that is at right angles to incoming fluxes. We also deduce that vorticity is most intense at $x/l = (2n-1)/(2m)$, $n \le m$, coinciding with pressure nodes, where the 'pumping-like' pressure-induced $\hat{u}$ has maximum amplitude. By comparison to the pressure, time-dependent vorticity is larger by $\mathcal{O}(S)$. This observation can be verified in the final formulation and stresses the appreciable role of vorticity.

C. Inviscid Vorticity

Equation (5.11) can now be used in conjunction with (5.6) to specify the separation eigenvalues:

$$\varpi_0\big|_{y=0} = -S\sin(k_m x) \equiv -S\sum_{n=0}^{\infty}\frac{(-1)^n (k_m x)^{2n+1}}{(2n+1)!}\,, \quad (5.12)$$

$$\lambda_n = 2n+1\,, c_n = -S(-1)^n (k_m)^{2n+1}/(2n+1)!\,, \quad (5.13)$$

whence

$$\varpi_0(x,y) = S\left\{\sum_{n=0}^{\infty}\frac{(-1)^n}{(2n+1)!}\left[-k_m x\cos(\tfrac{\pi}{2}y)\right]^{2n+1}\right\} \times\exp\left\{\tfrac{2}{\pi}\mathrm{i}S\ln\tan\left[\tfrac{\pi}{4}(1+y)\right]\right\}. \quad (5.14)$$

Recalling Taylor's mean flow stream function from Sec. II(C), we recognize that the infinite series between braces is a Sine function of Ψ. At the outset, we let $\mathrm{Z}(x,y) \equiv k_m\Psi(x,y)$, and simplify (5.14) into

$$\varpi_0(x,y) = S\sin(\mathrm{Z})\exp(-\mathrm{i}\Phi_0)\,, \quad (5.15)$$

where the temporal phase lead of the vortical wave is found to depend on

$$\Phi_0 = -\tfrac{2}{\pi}S\ln\tan\left[\tfrac{\pi}{4}(1+y)\right] = -\tfrac{2}{\pi}S\,\mathrm{gd}^{-1}(\tfrac{\pi}{2}y) \quad (5.16)$$

The inverse expression $\mathrm{gd}(\varsigma) = 2\arctan(\varsigma) - \frac{\pi}{2}$ relates to the Gudermannian function described in Abramowitz and Stegun.[45]

D. Inviscid Stream Function

We now resort to the time-dependent stream function $\overline{\boldsymbol{s}} = \psi\,\boldsymbol{k}$, where $\overline{\boldsymbol{u}} \equiv \nabla\times\overline{\boldsymbol{s}}$, to replace the velocity components via $\overline{u} = \partial\psi/\partial y$ and $\overline{v} = -\partial\psi/\partial x$. Starting with the vorticity equation,

$$\overline{\omega} = \frac{\partial\overline{v}}{\partial x} - \frac{\partial\overline{u}}{\partial y} = -\frac{\partial^2\psi}{\partial x^2} - \frac{\partial^2\psi}{\partial y^2}\,, \quad (5.17)$$

we then proceed heuristically by posing that ψ must possess the same axial dependence as $\overline{\omega}$. Since we shall be using successive approximations, we set $\psi_0 = \psi_c\varpi_0$, and substitute back into (5.17). Balancing leading-order terms implies that $\psi_c = \sigma^2\cos^2(\frac{\pi}{2}y)$ or

$$\psi_0 = \sigma\cos^2(\tfrac{\pi}{2}y)\sin[-k_m x\cos(\tfrac{\pi}{2}y)]\exp(-\mathrm{i}\Phi_0)\,. \quad (5.18)$$

Having determined the inviscid flow stream function, it follows that the companion velocity is

$$\overline{\boldsymbol{u}} = \left[\mathrm{i}\cos(\tfrac{\pi}{2}y)\sin(\mathrm{Z})\boldsymbol{i} + M\cos^3(\tfrac{\pi}{2}y)\cos(\mathrm{Z})\boldsymbol{j}\right]\exp(-\mathrm{i}\Phi_0). \quad (5.19)$$

E. Viscous Corrections

Subject to verification at the conclusion of this section, we state without proof that both $\overline{u}$ and $\overline{\omega}$ must possess the same axial dependence as their inviscid counterparts. This statement is implemented by setting

$$\overline{u}(x,y) = u_c(y)\sin(\mathrm{Z})\exp(-\mathrm{i}\Phi_0)\,,$$
$$\overline{\omega}(x,y) = \varpi_c(y)\sin(\mathrm{Z})\exp(-\mathrm{i}\Phi_0)\,, \quad (5.20)$$

where viscous correction multipliers, u_c and ϖ_c, must be evaluated. After substitution into the full vorticity transport equation, given by (5.2), several terms cancel out except for lower order terms and terms of $\mathcal{O}(S^2)$. Balancing leading-order terms demands that

$$\mathrm{d}\varpi_c/\mathrm{d}y + \xi\sec^3(\tfrac{\pi}{2}y)\varpi_c - \tfrac{\pi^2}{4}u_c = 0\,, \quad (5.21)$$

where $\xi = k_m^2/(M^3\overline{R})$ appears as a dynamic similarity parameter, chiefly in control of the viscous correction multiplier. In seeking a relationship between u_c and ϖ_c, we resort to (4.14) and find

$$u_c = \left[\mathrm{i}\sigma\cos(\tfrac{\pi}{2}y) + \xi\sigma^2\sec(\tfrac{\pi}{2}y)\right]\varpi_c\,. \quad (5.22)$$

Inserting this formula into (5.21) leads to an ordinary differential equation in ϖ_c:

$$\mathrm{d}\varpi_c/\mathrm{d}y + \left[\xi\sec^3(\tfrac{\pi}{2}y) - \mathrm{i}\sigma\tfrac{\pi^2}{4}\cos(\tfrac{\pi}{2}y)\right]\varpi_c = 0\,, \quad (5.23)$$

which, after some algebra, gives

$$\varpi_c(y) = C\exp\zeta\,, \quad (5.24)$$

where, by omitting the spurious imaginary argument in ζ of effective $\mathcal{O}(\sigma^2)$, we find

$$\zeta = -\xi\int_0^y v_0^{-3}(\tau)\mathrm{d}\tau = -\xi\int_0^y F^{-3}(\tau)\mathrm{d}\tau$$
$$= -\tfrac{1}{\pi}\xi\left[\ln\tan\tfrac{\pi}{4}(1+y) + \sec(\tfrac{\pi}{2}y)\tan(\tfrac{\pi}{2}y)\right]. \quad (5.25)$$

F. Corrected Vorticity

The complex constant of integration C can be evaluated from the vorticity boundary condition at the wall as specified by (5.11). Updating ϖ_c gives, at $\mathcal{O}(M,\sigma^2)$

$$C\left\{1-\xi\sigma^2\left[\zeta'(0)-\mathrm{i}\Phi_0{}'(0)\right]\right\}\sin\left[\mathrm{Z}(x,0)\right] \times\exp\left[\zeta(0)-\mathrm{i}\Phi_0(0)\right]=-S\sin(k_m x)\,, \qquad (5.26)$$

where

$$\zeta'(0)=-\xi\,;\ \Phi_0{}'(0)=-S\,;\ \zeta(0)=\Phi_0(0)=0\,. \qquad (5.27)$$

Direct substitution gives $C(1-\mathrm{i}\xi\sigma)=S+\mathcal{O}(\sigma^2)$. Choosing, henceforward, 'r' and 'i' superscripts to designate real and imaginary parts, we write

$$C^r=S^3/(S^2+\xi^2)\,,\quad C^i=\xi S^2/(S^2+\xi^2)\,. \qquad (5.28)$$

Backward substitution into (5.24), (5.20), and (4.10) yields, at last,

$$\tilde{\omega}(x,y,t)=C\sin(\mathrm{Z})\exp(\zeta-\mathrm{i}\Phi_0-\mathrm{i}k_m t)\,. \qquad (5.29)$$

G. Corrected Axial Velocity

In much the same way, the velocity corrective multiplier can be deduced from (5.22), viz.

$$u_c=\left[\mathrm{i}\sigma\cos(\tfrac{\pi}{2}y)+\xi\sigma^2\sec(\tfrac{\pi}{2}y)\right]C\exp\zeta\equiv\mathrm{i}B\exp\zeta\,, \qquad (5.30)$$

where

$$B^r=\sigma\left(C^r v_0+\xi\sigma C^i/v_0\right)\,,\ B^i=\sigma\left(C^i v_0-\xi\sigma C^r/v_0\right) \qquad (5.31)$$

so that $\tilde{\boldsymbol{u}}$ is soluble by backward substitution into (5.20) and (4.10). At length, we find that

$$\tilde{u}(x,y,t)=\mathrm{i}B\sin(\mathrm{Z})\exp(\zeta-\mathrm{i}\Phi_0-\mathrm{i}k_m t)\,. \qquad (5.32)$$

H. Normal Velocity

In principle, the normal component $\tilde{v}$ can be extracted from continuity. In practice, this may prove difficult unless we proceed heuristically by first proposing an *ansatz* of the form

$$\tilde{v}=g(y)\cos\left[-k_m x\cos(\tfrac{\pi}{2}y)\right]\exp(\zeta-\mathrm{i}\Phi_0-\mathrm{i}k_m t)\,. \qquad (5.33)$$

Later substitution into (4.5) furnishes $g(y)$. Setting $\partial\tilde{v}/\partial y\equiv-\partial\tilde{u}/\partial x$, we find, to leading order, $g=MBv_0^2$. Therefore,

$$\tilde{v}(x,y,t)=MBv_0^2\cos(\mathrm{Z})\exp(\zeta-\mathrm{i}\Phi_0-\mathrm{i}k_m t)\,, \qquad (5.34)$$

which lends support to the former stipulation contending that $\tilde{v}/\tilde{u}=\mathcal{O}(M)$.

I. The Real Time-Dependent Solution

Retracing our steps, the meaningful components of time-dependent axial and normal velocity are recapitulated below along with their vorticity companion.

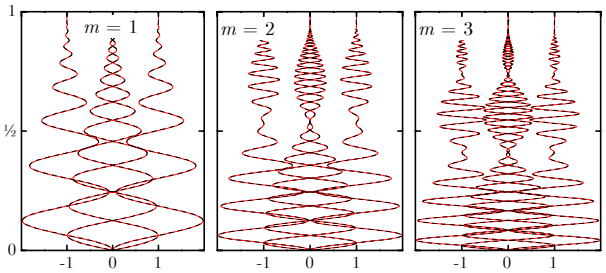

Fig. 2 A plot of u_1 versus y at four successive times separated by a $\pi/2$ phase difference. For every oscillation mode, profiles are depicted at the last harmonic pressure node, where $x/l=(2m-1)/2m$. Here $S=25m$ and $K=10^6 m$. To the accuracy of the graph, asymptotics (full lines) and numerics (broken lines) are indistinguishable.

$$u_1=\sin(k_m x)\sin(k_m t) -\left(B^r\sin\varphi-B^i\cos\varphi\right)\exp\zeta\sin(k_m x\cos\theta)\,, \qquad (5.35)$$

$$v_1=-Mv_0^2\left(B^r\cos\varphi+B^i\sin\varphi\right) \times\exp\zeta\cos(k_m x\cos\theta)\,, \qquad (5.36)$$

$$\omega_1=-\left(C^r\cos\varphi+C^i\sin\varphi\right)\exp\zeta\sin(k_m x\cos\theta) \qquad (5.37)$$

where

$$\theta=\tfrac{\pi}{2}y\,,\ \text{and}\ \ \varphi=k_m t-\frac{2}{\pi}S\ln\tan\left(\frac{\pi}{4}+\frac{\theta}{2}\right). \qquad (5.38)$$

Since the harmonic motion is, in essence, driven by the oscillatory pressure field, the first term in (5.35) can be envisaged as the inviscid response to the fluctuating pressure, and the second term can be interpreted as the viscous and vortical response that disappears asymptotically with increasing distance from the wall.

VI. Results and Comparisons

A. Numerical Verification

In order to gain confidence in the asymptotic formulas based on (5.35), we rely on computer-generated numerics and numerics combined with physical arguments. To that end, we use a shooting method to handle the two-point boundary value problem posing itself via (4.14) and the two auxiliary conditions described in Sec. IV(C). Careful choices of initial guesses and direction of integration across the channel are often necessary to ensure convergence. Our preference is to guess small nonzero values at the core and integrate backwards using a seventh order Runge-Kutta

scheme until the no-slip condition at the wall is fulfilled. Uniform steps, albeit very minute ones because of the desired accuracy, are found to be adequate for the most part. If the spatial grid is too coarse, then a numerical overflow occurs. Naturally, the numerical difficulty arises at large kinetic Reynolds numbers due to the failure of the integration routine or the divergence of the shooting scheme. This spurious numerical artifact, which can be prevented by grid refinement, is ascribed to the stiffness of the differential equation which is commensurate with the smallness of $1/K$. Continual spatial grid refinement is hence necessary at successive increases in K. The number of grid points needed for convergence varied in our monitored routine from 10,000 to 20,000,000 points, but no effort was made to optimize the number by employing non-uniform meshes. If this were done, far fewer grid points would have been necessitated near the wall, since the smaller steps are only required near the core to capture the exponentially depreciating vortical wavelength.

For typical values of the control parameters, the velocity's numerical solution is compared in Fig. 2 with its asymptotic counterpart evaluated from (5.35). For the first three oscillation modes, profiles are shown at four selected times of a complete cycle. For the fundamental mode, u_1 starts at zero at the wall, in satisfaction of the velocity-adherence condition, then undergoes a velocity overshoot of twice the irrotational core amplitude, before decaying gradually to its inviscid form. This overshoot near the wall is a well-known feature of oscillatory flows that has been first reported by Richardson.[46] The observed doubling in amplitude takes place when rotational and irrotational waves happen to be in phase. This virtual 100 percent amplification is far more intense than the 13 percent overshoot described in Rott[47] (cf. p. 402) and reported in laboratory experiments conducted, in the absence of wall injection, by Richardson,[46] and Richardson and Tyler.[40]

For higher modes, similar damped waves are observed in the upstream portion, $0 < x/l < 1/m$, delimited by the first internal velocity node. In the downstream portion, additional structures emerge. Specifically, a premature decay in the rotational wave is noted $m-1$ times downstream of the m^{th} velocity node. Such structures are depicted in Fig. 2 for $m = 2$ and 3, at the location of the last pressure node where irrotational velocity amplitudes are largest. Beyond these premature rotational velocity 'nodes,' so to speak, the vortical field recuperates some strength before resuming its normal depreciation. In order to justify the presence of such intellectually challenging rotational nodes, a characterization of the time-dependent vortical structure is deemed necessary. In the process, we attempt to capture the influence of varying wall injection and kinematic viscosity.

B. Time-Dependent Vortical Structure

For $m = 1$, formula (5.37) can be used to generate contour plots showing constant vorticity lines in percent of the maximum vorticity amplitude produced at the pressure nodes of the wall. When the frequency and kinematic viscosity are held constant, corresponding to a typical $K = 10^6$ value, the Strouhal number can be modified by an order of magnitude by reducing the injectant rate. The corresponding vortical structures are shown in Fig. 3, for $S = 10, 20$ and 100. In particular, we note in Fig. 3(a) the deeper vortical penetration with higher injection, and the downstream convection of vorticity, originating at the wall, that follows the mean flow streamlines. In Figs. 3(a-b), intense vorticity is still present at the downstream end measuring close to 100 percent of the maximum generated values at the wall. When injection is diminished in Fig. 3(c), the irrotational region anchored at the core broadens out, resulting in a substantial reduction in rotational depth. When this happens, intense vortical waves are entrained in the vicinity of the wall, and only weak vorticity persists at the downstream end.

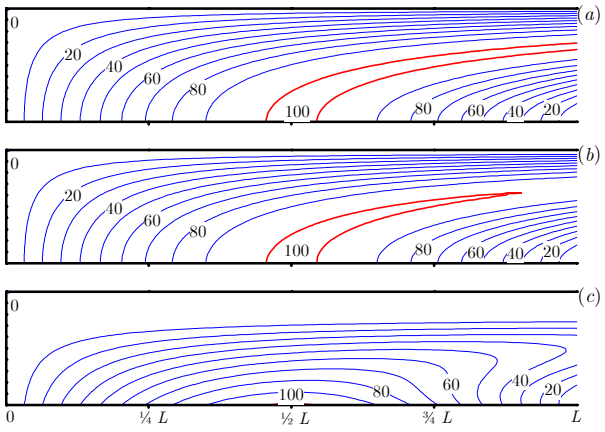

Fig. 3 Evenly spaced iso-vorticity lines shown in (a), (b) and (c) for $S =$ 10, 20 and 100. In all cases, $m = 1$ and $K = 10^6$. This variation can be ascribed to an order of magnitude depreciation in wall injection.

When, instead, v_w and k are held constant, the effect of kinematic viscosity can be extrapolated in a similar fashion by varying K. We find that, when viscosity is suppressed, as in Fig. 4, a wider and deeper spread of vorticity ensues. As such, one can envisage viscosity as an attenuation agent whose role is to resist the propagation of rotational waves. This is contrary to the role it plays in similar configurations with impermeable walls discussed, for example, in a survey by Rott[47] (cf. p. 397).

As the oscillation mode evolves to $m = 2, 3$ and 4, iso-vorticity lines begin exhibiting interesting structures. These are shown in Fig. 5 for typical values of the control parameters. In particular, these structures feature $(m-1)$ lines of zero vorticity amplitude, stemming from the harmonic pressure antinodes at the wall, for $m > 1$. These

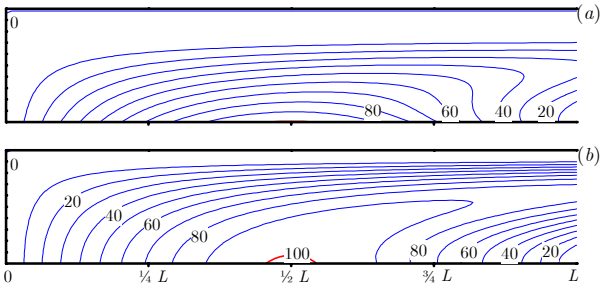

Fig. 4 Evenly spaced iso-vorticity lines shown in (a) and (b) for $K = 10^5$ and 10^6, when $m = 1$ and $S = 50$. This variation corresponds to an order of magnitude depreciation in the kinematic viscosity.

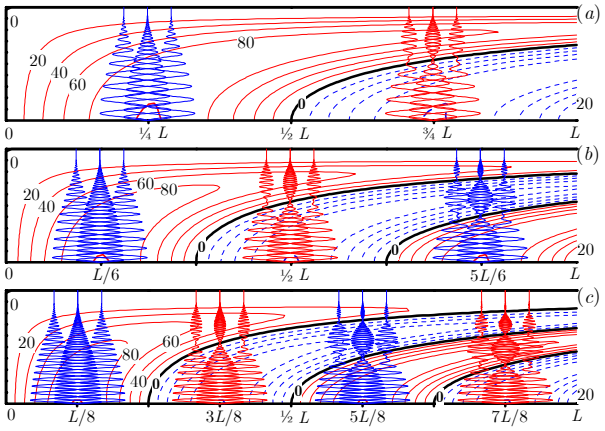

Fig. 5 Evenly spaced iso-vorticity lines shown in (a), (b) and (c) for the first three harmonics when $S = 25\,m$ and $K = 10^6\,m$. The oscillatory velocity u_1 is abbreviated by four evenly spread timelines depicted at select locations coinciding with harmonic pressure nodes.

irrotational streaks partition the channel into m zones characterized by alternating directions of particle rotation. When crossing these delineation lines, vorticity changes sign and therefore direction. This effect is captured graphically by switching between zones from full lines to broken lines. When time-dependent velocity profiles are superimposed at select axial locations, we find that the so-called rotational nodes in u_1 coincide precisely with the transverse location of the zero vorticity streaks. Apparently, as zero vorticity streaks drift downstream, they mark their local imprint by leaving rotational nodes in the velocity fields that they intersect. Similar effects are noted in Fig. 6 where an order of magnitude increase in viscosity is shown to hinder both vortical wave propagation depth and amplitude at higher modes as well.

C. Limiting Process Verification

In order to establish the lower limit that our mathematical model can tolerate for injection speeds, we reduce v_w until it drops below the diffusion speed, $v_d = \sqrt{2k\nu}$. The latter is associated with a Stokes' oscillatory field in a channel bounded by impermeable wall. This is necessitated by the insoluble singularity at $v_w = 0$ in our formulation. For example, when $v_w = v_d / \sqrt[3]{2}$, corresponding to $S = \sqrt{(K / \sqrt[3]{2})}$, and $R = 2^{1/6} h\sqrt{(k/\nu)}$, the Stokes number, defined here as $\lambda_S = \sqrt{(K/2)}$, will match the viscous parameter $\xi = S^3 / K$. When such conditions are established ($\xi = \lambda_S$), our asymptotic formulation

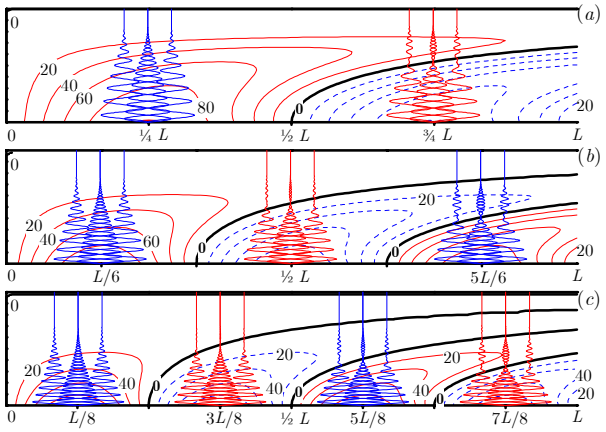

Fig. 6 Same as Fig. 5 except that here $K = 10^5\,m$, corresponding to an order of magnitude increase in kinematic viscosity.

can be compared to the known exact solution found, for example, in Rott[47] (cf. p. 402). The latter corresponds to an oscillating field in an infinitely long impermeable channel that is neither tailored to accommodate variations in the streamwise direction, nor oscillation modes brought about by the finite geometry. As such, it maintains a constant core amplitude. In order to reproduce this condition caused by 'pistons-at-infinity,' we compare solutions at $x/l = ½$ and $m = 1$, where the effects of finite body length are not felt. Results are shown in Fig. 7 at eight successive times separated by a $\pi/4$ phase difference. Apparently, our approximate solution embraces the exact solution when injection is suppressed. Thus, although it is possible to approximate the impermeable channel solution from ours, the converse is not true. This unexpected result may be attributed to the fact that Taylor's mean flow solution does match, near the wall, the more accurate formulation derived by Berman[1] for small injection. In our notation, the latter is given by $F = 1 - \frac{3}{2}y^2 + \frac{1}{2}y^3$, which resembles, near $y = 0$, Taylor's $F = \cos(\frac{\pi}{2}y) = 1 - \frac{\pi}{8}y^2 + \mathcal{O}(y^4)$.

D. Error Analysis

In arriving at the final asymptotic formulation set out in (5.35), a number of successive approximations were made that introduced uncertainty in the cumulative error entailed. Fortunately, the penultimate order verification of the error incurred in the derivation can be realized by applying a technique described by Bosley.[48] To that end, we define the maximum error E_m to be the maximum absolute difference between u_1 given asymptotically and u_1^n computed numerically. Then for every m, S, and K, we can calculate, over a complete oscillation cycle,

$$E_m(m,S,K) = \max_{\substack{0\le x\le l\\ 0\le y\le 1}} \left| u_1^n - u_1 \right| . \qquad (6.1)$$

Suspecting that the error could be of $\mathcal{O}(K^{-\alpha})$, we presuppose an error variation of the form

$$E_m(m,S,K) = \beta(m,S)(1/K)^{\alpha} , \qquad (6.2)$$

and determine the slope α from the log-log plot of E_m versus $1/K$. As depicted in Fig. 8 for the first two oscillation modes, the slope of the maximum error approaches one asymptotically irrespective of S. This result has been confirmed using the method of least-squares in decreasing ranges of ε, but is omitted here for brevity. The consistent asymptotic behavior is gratifying and, according to Bosley,[48] is indicative that our formulation is an honest and legitimate, uniformly valid expansion. This unexpected result shows that the error is, in fact, of $\mathcal{O}(\varepsilon)$. We could not have done any better since ε is the smallest naturally occurring perturbation parameter encountered heretofore. We do not forget, however, that the governing equation employed was correct to $\mathcal{O}(M)$, which ultimately sets the final error attendant on our idealization.

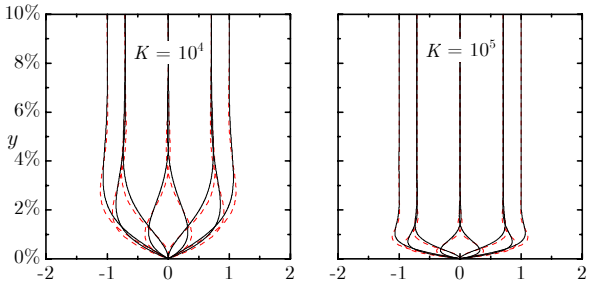

Fig. 7 Velocity profiles of u_1 shown at eight successive time intervals. Results are obtained from asymptotic predictions (broken lines) and the exact Stokes formula (full lines) at two arbitrary values of K and $\xi = \lambda_S$. In the absence of surface injection, the penetration of rotationality is more pronounced with higher viscosity (left).

VII. Concluding Remarks

In the present treatment, we have considered the effects of unsteadiness caused by small amplitude pressure oscillations about the classic Taylor flow in a porous channel. We have specifically excluded questions regarding hydrodynamic stability or turbulence in order to manage a basic, laminar solution for large wall injection. We have exploited a popular method that breaks down the

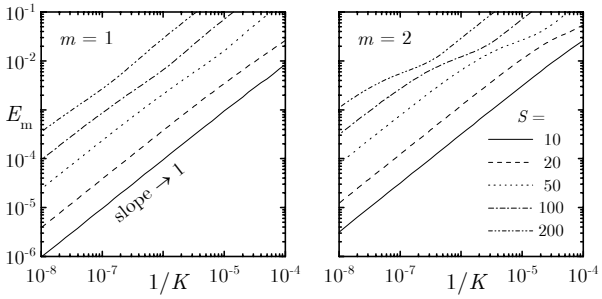

Fig. 8 Asymptotic behavior of the maximum absolute error between numerical and asymptotic predictions for the fundamental and first harmonic modes.

analysis into a steady, fundamentally nonlinear solution, and a superimposed, linearized, time-dependent part. The expressions arrived at were extruded from the vorticity transport equation using successive approximations. The formulas obtained were instrumental in revealing rich vortical structures that are by-products of mean and time-dependent flow interactions. They also revealed nondimensional parameters that control the flow character. By way of validation, comparisons to numerical solutions of the linearized Navier-Stokes equations were reassuring. Limiting process comparisons with the exact solution arising in the analogous setting with impermeable walls were also favorable. A formal assessment of the maximum error entailed at the conclusion of the asymptotic analysis revealed an unexpected bonus. The error was found to vary with the reciprocal of the kinetic Reynolds number, a practically large quantity. In a sense, we are pleased that this work increases our repertoire of known approximate formulations, and hope that the tactics presented here be exploited in other physical settings involving different configurations and boundary conditions.

References

[1]Berman, A. S., "Laminar Flow in Channels with Porous Walls," *Journal of Applied Physics,* Vol. 24, No. 9, 1953, pp. 1232-1235.

[2]Hiemenz, K., "Die Grenzschricht an einem in den gleichförmigen Flüssigkeitsstrom eingetauchten geraden Kreiszylinder," *Dingler's Polytechnisches Journal,* Vol. 326, No. 22, 1911, pp. 344-348.

[3]Berman, A. S., "Effects of Porous Boundaries on the Flow of Fluids in Systems with Various Geometries," *Proceedings of the Second United Nations International Conference on the Peaceful Uses of Atomic Energy, Series P/720,* Vol. 4, 1958, pp. 351-358.

[4]Sellars, J. R., "Laminar Flow in Channels with Porous Walls at High Suction Reynolds Numbers," *Journal of Applied Physics,* Vol. 26, No. 4, 1955, pp. 489-490.

[5]Terrill, R. M., "Laminar Flow in a Uniformly Porous Channel," *The Aeronautical Quarterly,* Vol. 15, 1964, pp. 299-310.

[6]Proudman, I., "An Example of Steady Laminar Flow at Large Reynolds Number," *Journal of Fluid Mechanics,* Vol. 9, No. 4, 1960, pp. 593-612.

[7]Morduchow, M., "On Laminar Flow through a Channel or Tube with Injection: Application of Method of Averages," *Quarterly Journal of Applied Mathematics,* Vol. 14, No. 4, 1956, pp. 361-368.

[8]White, F. M., Jr., Barfield, B. F., and Goglia, M. J., "Laminar Flow in a Uniformly Porous Channel," *Transactions of the American Society of Mechanical Engineers: Journal of Applied Mechanics, Series E,* Vol. 25, 1958, pp. 613-617.

[9]Taylor, G. I., "Fluid Flow in Regions Bounded by Porous Surfaces," *Proceedings of the Royal Society, London, Series A,* Vol. 234, No. 1199, 1956, pp. 456-475.

[10]Yuan, S. W., "Further Investigation of Laminar Flow in Channels with Porous Walls," *Journal of Applied Physics,* Vol. 27, No. 3, 1956, pp. 267-269.

[11]Terrill, R. M., "Laminar Flow in a Uniformly Porous Channel with Large Injection," *The Aeronautical Quarterly,* Vol. 16, 1965, pp. 323-332.

[12]Terrill, R. M., and Shrestha, G. M., "Laminar Flow through Channels with Porous Walls and with an Applied Transverse Magnetic Field," *Applied Scientific Research, Series B,* Vol. 11, 1964, pp. 134-144.

[13]Shrestha, G. M., "Singular Perturbation Problems of Laminar Flow in a Uniformly Porous Channel in the Presence of a Transverse Magnetic Field," *Quarterly Journal of Mechanics and Applied Mathematics,* Vol. 20, No. 2, 1967, pp. 233-246.

[14]Terrill, R. M., and Shrestha, G. M., "Laminar Flow Through Parallel and Uniformly Porous Walls of Different Permeability," *Journal of Applied Mathematics and Physics (ZAMP),* Vol. 16, 1965, pp. 470-482.

[15]Shrestha, G. M., and Terrill, R. M., "Laminar Flow with Large Injection Through Parallel and Uniformly Porous Walls of Different Permeability," *Quarterly Journal of Mechanics and Applied Mathematics,* Vol. 21, No. 4, 1968, pp. 413-432.

[16]Cox, S. M., "Two-dimensional Flow of a Viscous Fluid in a Channel with Porous Walls," *Journal of Fluid Mechanics,* Vol. 227, 1991, pp. 1-33.

[17]Brady, J. F., and Acrivos, A., "Steady Flow in a Channel or Tube with an Accelerating Surface Velocity. An Exact Solution to the Navier-Stokes Equations with Reverse Flow," *Journal of Fluid Mechanics,* Vol. 112, 1981, pp. 127-150.

[18]Watson, E. B. B., Banks, W. H. H., Zaturska, M. B., and Drazin, P. G., "On Transition to Chaos in Two-dimensional Channel Flow Symmetrically Driven by Accelerating Walls," *Journal of Fluid Mechanics,* Vol. 212, 1990, pp. 451-485.

[19]Watson, P., Banks, W. H. H., Zaturska, M. B., and Drazin, P. G., "Laminar Channel Flow Driven by Accelerating Walls," *European Journal of Applied Mathematics,* Vol. 2, 1991, pp. 359-385.

[20]Varapaev, V. N., and Yagodkin, V. I., "Flow Stability in a Channel with Porous Walls," *Fluid Dynamics (Izvestiya Akademii Nauk SSSR, Meckanika Zhidkosti i Gaza),* Vol. 4, No. 5, 1969, pp. 91-95.

[21]Raithby, G. D., and Knudsen, D. C., "Hydrodynamic Development in a Duct with Suction and Blowing," *Transactions of the American Society of Mechanical Engineers: Journal of Applied Mechanics, Series E,* Vol. 41, 1974, pp. 896-902.

[22]Hocking, L. M., "Non-linear Instability of the Asymptotic Suction Velocity Profile," *Quarterly Journal*

of Mechanics and Applied Mathematics, Vol. 28, No. 3, 1975, pp. 341-353.

[23]Sviridenkov, A. A., and Yagodkin, V. I., "Flow in the Initial Sections of Channels with Permeable Walls," *Fluid Dynamics (Izvestiya Akademii Nauk SSSR, Meckanika Zhidkosti i Gaza),* Vol. 11, No. 5, 1976, pp. 689-693.

[24]Brady, J. F., "Flow Development in a Porous Channel or Tube," *The Physics of Fluids,* Vol. 27, No. 5, 1984, pp. 1061-1067.

[25]Durlofsky, L., and Brady, J. F., "The Spatial Stability of a Class of Similarity Solutions," *The Physics of Fluids,* Vol. 27, No. 5, 1984, pp. 1068-1076.

[26]Robinson, W. A., "The Existence of Multiple Solutions for the Laminar Flow in a Uniformly Porous Channel with Suction at Both Walls," *Journal of Engineering Mathematics,* Vol. 10, No. 1, 1976, pp. 23-40.

[27]Skalak, F. M., and Wang, C.-Y., "On the Nonunique Solutions of Laminar Flow Through a Porous Tube or Channel," *SIAM Journal on Applied Mathematics,* Vol. 34, No. 3, 1978, pp. 535-544.

[28]Shih, K.-G., "On the Existence of Solutions of an Equation Arising in the Theory of Laminar Flow in a Uniformly Porous Channel with Injection," *SIAM Journal on Applied Mathematics,* Vol. 47, No. 3, 1987, pp. 526-533.

[29]Hastings, S. P., Lu, C., and MacGillivray, A. D., "A Boundary Value Problem with Multiple Solutions from the Theory of Laminar Flow," *SIAM Journal on Mathematical Analysis,* Vol. 23, No. 1, 1992, pp. 201-208.

[30]Lu, C., MacGillivray, A. D., and Hastings, S. P., "Asymptotic Behaviour of Solutions of a Similarity Equation for Laminar Flows in Channels with Porous Walls," *IMA Journal of Applied Mathematics,* Vol. 49, 1992, pp. 139-162.

[31]MacGillivray, A. D., and Lu, C., "Asymptotic Solution of a Laminar Flow in a Porous Channel with Large Suction: A Nonlinear Turning Point Problem," *Methods and Applications of Analysis,* Vol. 1, No. 2, 1994, pp. 229-248.

[32]Lu, C., "On the Asymptotic Solution of Laminar Channel Flow with Large Suction," *SIAM Journal on Mathematical Analysis,* Vol. 28, No. 5, 1997, pp. 1113-1134.

[33]Zaturska, M. B., Drazin, P. G., and Banks, W. H. H., "On the Flow of a Viscous Fluid Driven Along a Channel by Suction at Porous Walls," *Fluid Dynamics Research,* Vol. 4, No. 3, 1988, pp. 151-178.

[34]Taylor, C. L., Banks, W. H. H., Zaturska, M. B., and Drazin, P. G., "Three-dimensional Flow in a Porous Channel," *Quarterly Journal of Mechanics and Applied Mathematics,* Vol. 44, No. 1, 1991, pp. 105-133.

[35]Ma, Y., Van Moorhem, W. K., and Shorthill, R. W., "Innovative Method of Investigating the Role of Turbulence in the Velocity Coupling Phenomenon," *Journal of Vibration and Acoustics-Transactions of the ASME,* Vol. 112, No. 4, 1990, pp. 550-555.

[36]Ma, Y., Van Moorhem, W. K., and Shorthill, R. W., "Experimental Investigation of Velocity Coupling in Combustion Instability," *Journal of Propulsion and Power,* Vol. 7, No. 5, 1991, pp. 692-699.

[37]Barron, J., Majdalani, J., and Van Moorhem, W. K., "A Novel Investigation of the Oscillatory Field over a Transpiring Surface," AIAA Paper 98-2694, June 1998.

[38]Avalon, G., Casalis, G., and Griffond, J., "Flow Instabilities and Acoustic Resonance of Channels with Wall Injection," AIAA Paper 98-3218, July 1998.

[39]Casalis, G., Avalon, G., and Pineau, J.-P., "Spatial Instability of Planar Channel Flow with Fluid Injection Through Porous Walls," *The Physics of Fluids,* Vol. 10, No. 10, 1998, pp. 2558-2568.

[40]Richardson, E. G., and Tyler, E., "The Transverse Velocity Gradient Near the Mouths of Pipes in which an Alternating or Continuous Flow of Air is Established," *Proceedings of the Royal Society, London, Series A,* Vol. 42, No. 1, 1929, pp. 1-15.

[41]Lighthill, M. J., "The Response of Laminar Skin Friction and Heat Transfer to Fluctuations in the Stream Velocity," *Proceedings of the Royal Society, London, Series A,* Vol. 224, 1954, pp. 1-23.

[42]Sommerfeld, A., *Mechanics of Deformable Bodies*, *Lectures on Theoretical Physics*, Sec. 20, Vol. IV, Academic Press, New York, 1950, pp. 147-154.

[43]Chu, B.-T., and Kovásznay, L. S. G., "Non-linear Interactions in a Viscous Heat-conducting Compressible Gas," *Journal of Fluid Mechanics,* Vol. 3, 1957, pp. 494-514.

[44]Carrier, B. T., and Carlson, F. D., "On the Propagation of Small Disturbances in a Moving Compressible Fluid," *Quarterly of Applied Mathematics,* Vol. 4, No. 1, 1946, pp. 1-12.

[45]Abramowitz, M., and Stegun, I. A., *Handbook of Mathematical Functions*, National Bureau of Standards, 1964, pp. 77.

[46]Richardson, E. G., "The Amplitude of Sound Waves in Resonators," *Proceedings of the Physical Society, London,* Vol. 40, No. 27, 1928, pp. 206-220.

[47]Rott, N., *Theory of Time-Dependent Laminar Flows*, *High Speed Aerodynamics and Jet Propulsion – Theory of Laminar Flows*, Sec. D, Vol. IV, edited by F. K. Moore, Princeton University Press, Princeton, New Jersey, 1964, pp. 395-438.

[48]Bosley, D. L., "A Technique for the Numerical Verification of Asymptotic Expansions," *SIAM Review,* Vol. 38, No. 1, 1996, pp. 128-135.